Water Waves (2021) 3:127–152
https://doi.org/10.1007/s42286-020-00029-7

ORIGINAL ARTICLE

Normal Form Transformations and Dysthe's Equation for the Nonlinear Modulation of Deep-Water Gravity Waves

Walter Craig[1] · Philippe Guyenne[2] · Catherine Sulem[3]

Received: 23 October 2019 / Accepted: 6 March 2020 / Published online: 24 March 2020

Abstract
A new Hamiltonian version of Dysthe's equation is derived for two-dimensional weakly modulated gravity waves on deep water. A key ingredient in this derivation is a Birkhoff normal form transformation that eliminates all non-resonant cubic terms and allows for a refined reconstruction of the free surface. This modulational approximation is tested against numerical solutions of the classical Dysthe's equation and against direct numerical simulations of Euler's equations for nonlinear water waves. Very good agreement is found in the context of Benjamin–Feir instability of Stokes waves, for which an analysis is provided. An extension of our Hamiltonian model incorporating exact linear dispersion as well as an alternate spatial form are also proposed.

Keywords Deep water · Dirichlet–Neumann operator · Dysthe's equation · Gravity waves · Hamiltonian systems · Modulation theory · Normal forms

1 Introduction

Modulation theory has been an effective tool for the asymptotic modeling and analysis of surface gravity waves in a weakly nonlinear scaling regime. Two limiting regimes of interest are the shallow-water regime where waves are viewed as mild modulations

Walter Craig passed away on January 18, 2019.

In memory of Walter Craig, outstanding mathematician and dear friend.

✉ Philippe Guyenne
guyenne@udel.edu

Catherine Sulem
sulem@math.utoronto.ca

[1] Department of Mathematics and Statistics, McMaster University, Hamilton, ON L8S 4K1, Canada

[2] Department of Mathematical Sciences, University of Delaware, Newark, DE 19716-2553, USA

[3] Department of Mathematics, University of Toronto, Toronto, ON M5S 2E4, Canada

of the uniform mean flow, and the deep-water regime where approximate solutions are sought in the form of mild modulations of monochromatic waves. The former case leads to Boussinesq-type equations (and their variants) for which solutions are typically localized in space [8,12]. The present study is focused on the latter case where a modulational Ansatz makes it possible to derive reduced models for the wave envelope. A well-known example is the nonlinear Schrödinger (NLS) equation, which emerges from the first nontrivial terms in the perturbation calculations [1,38]. This equation has been extensively studied owing to its many mathematical properties and the fact that it is a canonical model for nonlinear dispersive waves in many other areas (e.g. optics, plasma physics, etc.) [32]. Another example is the Davey–Stewartson system which describes wave modulation on finite depth in higher space dimensions [2,13,16].

Higher order envelope equations have also drawn much attention from the scientific community. In the water wave setting, the next-order correction to the NLS equation has first been proposed by Dysthe [22] via a multiple-scale analysis. His model has then been rederived and extended by many other investigators to allow for, e.g. broader banded waves, exact linear dispersion, or time-series comparison with laboratory experiments [21,35,36,39]. In particular, Stiassnie [31] showed that Dysthe's equation can also be derived via the mode coupling approach of Zakharov [38]. These higher order models exhibit improved stability properties for finite-amplitude waves, including a Doppler shift due to the wave-induced mean flow. Consistent with direct numerical simulations, they also predict an asymmetric evolution of the sideband modes during modulational instability, which is a phenomenon that is not described by modeling with the NLS equation. Despite this progress, early versions of Dysthe's equation share a fundamental shortcoming: they are not Hamiltonian whereas the original water wave equations are. From a modeling point of view, it is desirable that a reduced model inherits important properties of the original system.

This issue has recently been addressed by Craig et al. [13,14] and Gramstad and Trulsen [23] who proposed Hamiltonian versions of Dysthe's equation. Gramstad and Trulsen [23] used Krasitskii's [26] Hamiltonian version of Zakharov's equation as a basis for their modulational analysis, while Craig et al. [13,14] used a Taylor series expansion of the Dirichlet–Neumann operator and applied a set of canonical transformations together with homogenization techniques to the original Hamiltonian formulation of the water wave problem.

Because the derivation of envelope equations relies on a clear separation between resonant and non-resonant wave interactions and on a subtle elimination of non-resonant terms, it is important to obtain a procedure that is valid for wave evolution over sufficiently long times, on the order $O(\varepsilon^{-2})$ where ε is a measure of the wave steepness. For Hamiltonian systems, this elimination can be performed in a natural way via canonical normal form transformations [3,4,7,25]. Such a transformation has recently been constructed by Craig and Sulem [18] in a Sobolev space setting to eliminate all non-resonant cubic terms from the Hamiltonian of two-dimensional gravity waves on deep water, resulting in a simple and elegant normal form for the reduced problem.

In the present study, we combine results from [13,14,18] to derive a new Hamiltonian version of Dysthe's equation for deep-water gravity waves, based on the straightforward method of canonical transformations as mentioned above, but imple-

mented after applying the normal form transformation that eliminates non-resonant cubic terms. Our new version of the envelope equations is similar to that found in [13], modulo slightly different coefficients for nonlinear terms. A careful determination of the envelope equation turns out to be crucial for closely capturing the wave dynamics in this modulational regime. We test our Hamiltonian Dysthe's equation against predictions by the classical Dysthe's equation, comparing both models to direct numerical simulations of Euler's equations for free-surface water waves. Given the high precision of our numerical simulations of the full equations, this test constitutes a verification of both the original Dysthe's equation and our Hamiltonian version. To our knowledge, this is the first time here that such a verification of the Hamiltonian Dysthe's equation is performed. Earlier studies [13,23] did not report any numerical result. Craig et al. [14] showed preliminary numerical simulations of their Hamiltonian model but did not conduct any comparison with predictions by Euler's equations.

Of particular interest is the development of modulational instability for a perturbed Stokes wave, for which we present a linear stability analysis and a numerical investigation. In this regard, we also pay attention to the post-processing step of reconstructing the free surface from the wave envelope, which is another key factor influencing the model's performance. Inspired by the recent work of Craig and Sulem [18], we propose a new non-perturbative approach for surface reconstruction based on the numerical solution of a nonlinear partial differential equation (PDE). In doing so, higher order harmonic components of the wave spectrum are automatically generated by the carrier wave via nonlinear interactions. This differs from the traditional procedure where the free surface is reconstructed perturbatively in terms of a Stokes expansion [30,35]. Furthermore, we provide extensions of our high-order envelope equation to cases where exact linear dispersion is retained [36] and where the model is rewritten in an alternate spatial form to facilitate possible comparison with laboratory experiments [27].

The question of rigorous justification of the modulational Ansatz has two elements: first one needs a sufficiently long-time existence theorem, on the order $O(\varepsilon^{-2})$, for solutions of Euler's equations, and second, the latter should be well approximated by solutions of the NLS equation. Some progress has been made since the work by Craig et al. [19] who addressed the question of how well the constructed modulational Ansatz approximates solutions of Euler's equations, but did not provide any long-time existence result. Totz and Wu [33,34] proved the validity of the NLS approximation for the two- and three-dimensional water wave problem in a channel of infinite depth. The finite-depth case involves additional difficulties and was investigated by Düll et al. [20]. Due to the loss of smoothness in normal form transformations, estimates were performed in spaces of analytic functions. We also mention recent results by Berti et al. [5] who proved a long-time existence result for water waves in the two-dimensional periodic setting with infinite depth.

This paper is organized as follows. Section 2 recalls the basic mathematical formulation for two-dimensional gravity waves on deep water, including the Hamiltonian form of the governing equations. Sections 3 and 4 describe the main steps in our Hamiltonian perturbation approach, including the normal form transformation to eliminate all non-resonant cubic terms and the modulation Ansatz to specify the special near-monochromatic form of solutions in this scaling regime. Section 5 presents our new Hamiltonian models in cases with truncated and exact linear dispersion, and the corre-

sponding procedure for surface reconstruction is discussed in Sect. 6. The spatial form of our truncated envelope equation is introduced in Sect. 7, and the stability analysis is outlined in Sect. 8. Numerical results are shown in Sect. 9 where the Hamiltonian model is compared to the classical Dysthe's equation and the full water wave equations. Finally, concluding remarks are given in Sect. 10.

2 Hamiltonian Formulation

We consider the evolution of a free surface $\{y = \eta(x,t)\}$ on top of a two-dimensional fluid of infinite depth

$$S(\eta) = \{x \in \mathbb{R}, -\infty < y < \eta(x,t)\},$$

under the influence of gravity. Here (x, y) denote the horizontal and vertical coordinates, respectively, and t represents time. In the version of Euler's equations for an incompressible, inviscid and irrotational flow with a free surface, the velocity potential $\varphi(x, y, t)$ satisfies the boundary value problem

$$\nabla^2\varphi = 0 \quad \text{in} \quad S(\eta), \tag{1}$$

$$\partial_t\eta + (\partial_x\eta)(\partial_x\varphi) - \partial_y\varphi = 0 \quad \text{at} \quad y = \eta(x,t), \tag{2}$$

$$\partial_t\varphi + \frac{1}{2}|\nabla\varphi|^2 + g\eta = 0 \quad \text{at} \quad y = \eta(x,t), \tag{3}$$

$$\partial_y\varphi \to 0 \quad \text{as} \quad y \to -\infty, \tag{4}$$

where g denotes the acceleration due to gravity and $\nabla = (\partial_x, \partial_y)^\top$.

Following Craig and Sulem [17], the dimensionality of the Laplace problem (1)–(4) can be reduced by considering surface quantities as unknown variables. This is accomplished by introducing the Dirichlet–Neumann operator (DNO)

$$G(\eta)\xi = (-\partial_x\eta, 1)^\top \cdot \nabla\varphi\big|_{y=\eta}, \tag{5}$$

which takes Dirichlet data $\xi(x,t) = \varphi(x, \eta(x,t), t)$ at the free surface, solves the Laplace equation (1) for φ subject to (4), and returns the corresponding Neumann data (i.e. the normal velocity at the free surface). As a result, Eqs. (1)–(4) reduce to

$$\partial_t\eta = G(\eta)\xi, \tag{6}$$

$$\partial_t\xi = -g\eta - \frac{1}{2\left(1 + (\partial_x\eta)^2\right)}\left[(\partial_x\xi)^2 - (G(\eta)\xi)^2 - 2(\partial_x\eta)(\partial_x\xi)G(\eta)\xi\right], \tag{7}$$

which are Hamiltonian equations for the two conjugate variables η and ξ in Zakharov's formulation of the water wave problem [17,38]. These can be expressed in canonical form

$$\partial_t\begin{pmatrix}\eta\\ \xi\end{pmatrix} = J\begin{pmatrix}\delta_\eta H\\ \delta_\xi H\end{pmatrix} = \begin{pmatrix}0 & 1\\ -1 & 0\end{pmatrix}\begin{pmatrix}\delta_\eta H\\ \delta_\xi H\end{pmatrix}, \tag{8}$$

where the 2×2 matrix J represents the symplectic structure of the system, and the Hamiltonian

$$H(\eta, \xi) = \frac{1}{2} \int \left[\xi G(\eta) \xi + g\eta^2 \right] \mathrm{d}x, \tag{9}$$

corresponds to the total energy, which is conserved over time. For simplicity, the domain of integration is not specified in (9) but hereafter it is understood that all integrals are evaluated over $\mathbb{R}$.

It is known that the DNO is an analytic function of η provided the free surface has sufficient regularity [6], which implies that the DNO can be written in terms of a convergent Taylor series expansion

$$G(\eta) = \sum_{j=0}^{\infty} G_j(\eta), \tag{10}$$

about the quiescent state $\eta = 0$. Each Taylor term G_j is homogeneous of degree j in η and can be determined recursively [17]. For example, the first few terms are

$$\begin{aligned} G_0 &= |D|, \\ G_1(\eta) &= D\eta D - G_0 \eta G_0, \\ G_2(\eta) &= -\frac{1}{2} \left(|D|^2 \eta^2 G_0 + G_0 \eta^2 |D|^2 - 2 G_0 \eta G_0 \eta G_0 \right), \end{aligned}$$

where $D = -\mathrm{i}\partial_x$ (so that its Fourier symbol is k). The reader may refer to [9,11,12,15, 24,37] for applications of this formulation to long-wave perturbation calculations as well as direct numerical simulations of nonlinear waves on uniform or variable depth.

Let us decompose $H = H_2 + H_3 + H_4 + \cdots$, where

$$\begin{aligned} H_2(\eta, \xi) &= \frac{1}{2} \int \left(\xi G_0 \xi + g\eta^2 \right) \mathrm{d}x, \\ H_3(\eta, \xi) &= \frac{1}{2} \int \xi G_1(\eta) \xi \, \mathrm{d}x = \frac{1}{2} \int \xi \left(D\eta D - G_0 \eta G_0 \right) \xi \, \mathrm{d}x, \\ &= -\frac{1}{2} \int \eta \left[(D\xi)^2 + (G_0 \xi)^2 \right] \mathrm{d}x, \\ H_4(\eta, \xi) &= \frac{1}{2} \int \xi G_2(\eta) \xi \, \mathrm{d}x \\ &= -\frac{1}{4} \int \xi \left(|D|^2 \eta^2 G_0 + G_0 \eta^2 |D|^2 - 2 G_0 \eta G_0 \eta G_0 \right) \xi \, \mathrm{d}x, \\ &= -\frac{1}{2} \int \eta \left[\eta (G_0 \xi)(D^2 \xi) - (G_0 \xi) G_0 (\eta G_0 \xi) \right] \mathrm{d}x, \end{aligned}$$

represent the quadratic, cubic and quartic contributions respectively, in terms of the dependent variables. The first one, H_2, describes linear dynamics while H_3 and H_4 describe nonlinear mechanisms of three-wave and four-wave interactions, respectively.

Following Craig et al. [13,14], our Hamiltonian approach to deriving envelope equations for the modulation of weakly nonlinear wave packets involves various transformations that approximate the original Hamiltonian (9) of the system and adjust the symplectic structure (8) accordingly. These transformations are discussed in the next sections.

3 Normal Form Transformations

Because three-wave resonances do not occur in the context of deep-water gravity waves, the Hamiltonian $H(\eta, \xi)$ can be simplified by eliminating all cubic terms through an appropriate canonical transformation, as these are not essential to the wave dynamics [26]. This approach falls within the general theory of normal form transformations for Hamiltonian systems and has been successfully applied to the water wave problem since the pioneering work of Zakharov [38]. Birkhoff normal form up to a given order m is the result of a canonical change of variables, so that the Taylor expansion of the transformed Hamiltonian up to order m contains only resonant terms.

In the two-dimensional setting with infinite depth [18], the normal form transformation for $m = 3$ can be constructed as the flow at $s = -1$ governed by the vector field

$$\partial_s \begin{pmatrix} \eta \\ \xi \end{pmatrix} = \begin{pmatrix} 0 & 1 \\ -1 & 0 \end{pmatrix} \begin{pmatrix} \delta_\eta K_3 \\ \delta_\xi K_3 \end{pmatrix}, \tag{11}$$

for some auxiliary Hamiltonian K_3, and with initial condition at $s = 0$ corresponding to the original physical variables (η, ξ). Expressing the new Hamiltonian in terms of a Taylor expansion about $s = 0$,

$$\begin{aligned} H(\eta,\xi)\big|_{s=-1} &= H(\eta,\xi)\big|_{s=0} - \frac{\mathrm{d}H}{\mathrm{d}s}(\eta,\xi)\big|_{s=0} + \frac{1}{2}\frac{\mathrm{d}^2 H}{\mathrm{d}s^2}(\eta,\xi)\big|_{s=0} + \cdots, \\ &= H(\eta,\xi)\big|_{s=0} - \{K_3, H\}(\eta,\xi)\big|_{s=0} + \frac{1}{2}\{K_3, \{K_3, H\}\}(\eta,\xi)\big|_{s=0} + \cdots, \\ &= H_2(\eta,\xi)\big|_{s=0} + H_3(\eta,\xi)\big|_{s=0} + H_4(\eta,\xi)\big|_{s=0} - \{K_3, H_2\}(\eta,\xi)\big|_{s=0} \\ &\quad - \{K_3, H_3\}(\eta,\xi)\big|_{s=0} + \frac{1}{2}\{K_3, \{K_3, H_2\}\}(\eta,\xi)\big|_{s=0} + \cdots, \end{aligned}$$

where K_3 is homogeneous of degree 3, H_n is homogeneous of degree n and $\{K_3, H_n\}$ is of degree $n + 1$, it follows that all cubic terms are eliminated, i.e.

$$H_3(\eta,\xi)\big|_{s=0} - \{K_3, H_2\}(\eta,\xi)\big|_{s=0} = 0, \tag{12}$$

provided

$$K_3(\eta,\xi) = \frac{1}{2}\int (-\mathrm{i}\,\mathrm{sgn}(D)\eta)^2\, |D|\xi\, \mathrm{d}x.$$

The operator $-\mathrm{i}\,\mathrm{sgn}(D)$ may be viewed as the Hilbert transform associated with the infinite lower half-plane. Terms in the above expansion are related to Poisson brackets by virtue of

$$\begin{aligned}\frac{\mathrm{d}H}{\mathrm{d}s} &= \int \left[(\delta_\eta H)(\partial_s \eta) + (\delta_\xi H)(\partial_s \xi)\right]\mathrm{d}x = \int \left[(\delta_\eta H)(\delta_\xi K_3) - (\delta_\xi H)(\delta_\eta K_3)\right]\mathrm{d}x,\\ &= \{K_3, H\}\,.\end{aligned}$$

A more familiar form of (11) can be obtained by introducing

$$\begin{pmatrix}\widetilde{\eta}\\ \widetilde{\xi}\end{pmatrix} = P_0\begin{pmatrix}\eta\\ \xi\end{pmatrix} = \begin{pmatrix}-\mathrm{i}\,\mathrm{sgn}(D) & 0\\ 0 & -\mathrm{i}\,\mathrm{sgn}(D)\end{pmatrix}\begin{pmatrix}\eta\\ \xi\end{pmatrix}, \tag{13}$$

in which case

$$K_3(\widetilde{\eta}, \widetilde{\xi}) = \frac{1}{2}\int \widetilde{\eta}^2 \partial_x \widetilde{\xi}\,\mathrm{d}x, \tag{14}$$

and

$$\partial_s\begin{pmatrix}\widetilde{\eta}\\ \widetilde{\xi}\end{pmatrix} = J_0\begin{pmatrix}\delta_{\widetilde{\eta}} K_3\\ \delta_{\widetilde{\xi}} K_3\end{pmatrix} = \begin{pmatrix}0 & -1\\ 1 & 0\end{pmatrix}\begin{pmatrix}\delta_{\widetilde{\eta}} K_3\\ \delta_{\widetilde{\xi}} K_3\end{pmatrix}, \tag{15}$$

following upon the adjustment $J_0 = P_0 J P_0^\top = -J$. The first equation for $\widetilde{\eta}$ is Burgers' equation

$$\partial_s \widetilde{\eta} - \widetilde{\eta}\partial_x \widetilde{\eta} = 0,$$

while the second equation for $\widetilde{\xi}$,

$$\partial_s \widetilde{\xi} - \widetilde{\eta}\partial_x \widetilde{\xi} = 0,$$

is its linearization along Burgers' flow. The new Hamiltonian, after this normal form transformation, reduces to

$$\begin{aligned}H &= H_2(\eta, \xi) + H_4(\eta, \xi) - \{K_3, H_3\}(\eta, \xi) + \frac{1}{2}\{K_3, \{K_3, H_2\}\}(\eta, \xi) + R_5,\\ &= H_2(\eta, \xi) + H_4(\eta, \xi) - \frac{1}{2}\{K_3, H_3\}(\eta, \xi) + R_5,\\ &= H_2(\eta, \xi) + H_4(\eta, \xi) - H_4(-\mathrm{i}\,\mathrm{sgn}(D)\eta, \xi) + R_5,\end{aligned} \tag{16}$$

where the leading nonlinear contributions are now quartic terms. We have used (12) together with the fact that

$$\frac{1}{2}\{K_3, H_3\}(\eta, \xi) = \frac{1}{2}\int \xi G_2(-\mathrm{i}\,\mathrm{sgn}(D)\eta)\xi\,\mathrm{d}x = H_4(-\mathrm{i}\,\mathrm{sgn}(D)\eta, \xi),$$

as shown by Craig and Sulem [18, Theorem 4.1]. Because this is a canonical transformation, it preserves the symplectic structure J in (8). More details on Birkhoff normal forms for water waves can be found in [5,7,18,38]. We remark that it is continuous in a suitably small neighborhood of $(\widetilde{\eta}, \widetilde{\xi}) = 0$ in Sobolev spaces H^r $(r > 1/2)$, but it is not differentiable with respect to $(\widetilde{\eta}, \widetilde{\xi})$ and, therefore, is not a flow in the classical sense.

4 Modulational Ansatz

We now set the stage to describe the scaling regime that encodes the special form of wave solutions that we are interested in. First, we transform to complex symplectic coordinates $z(x,t)$ and $\overline{z}(x,t)$ as defined by

$$\begin{pmatrix} z \\ \overline{z} \end{pmatrix} = P_1 \begin{pmatrix} \eta \\ \xi \end{pmatrix} = \frac{1}{\sqrt{2}} \begin{pmatrix} a(D) & \mathrm{i}a^{-1}(D) \\ a(D) & -\mathrm{i}a^{-1}(D) \end{pmatrix} \begin{pmatrix} \eta \\ \xi \end{pmatrix}, \tag{17}$$

where

$$a(D) = \sqrt[4]{\frac{g}{G_0}},$$

and the symbol $\bar{\cdot}$ stands for complex conjugation. As a result, system (8) becomes

$$\partial_t \begin{pmatrix} z \\ \overline{z} \end{pmatrix} = J_1 \begin{pmatrix} \delta_z H \\ \delta_{\overline{z}} H \end{pmatrix} = \begin{pmatrix} 0 & -\mathrm{i} \\ \mathrm{i} & 0 \end{pmatrix} \begin{pmatrix} \delta_z H \\ \delta_{\overline{z}} H \end{pmatrix},$$

with the transformed symplectic structure $J_1 = P_1 J P_1^\top$.

The next step introduces our modulational Ansatz

$$\begin{pmatrix} u \\ \overline{u} \end{pmatrix} = P_2 \begin{pmatrix} z \\ \overline{z} \end{pmatrix} = \varepsilon^{-1} \begin{pmatrix} e^{-\mathrm{i}k_0 x} & 0 \\ 0 & e^{\mathrm{i}k_0 x} \end{pmatrix} \begin{pmatrix} z \\ \overline{z} \end{pmatrix}, \tag{18}$$

a translation in Fourier space variables, which is to say that we are looking for solutions in the form of near-monochromatic waves with carrier wavenumber $k_0 > 0$ and with slowly varying complex envelope $u(X,t)$ depending on $X = \varepsilon x$. The small dimensionless parameter $\varepsilon \sim k_0 A_0 \ll 1$ is a measure of the wave steepness (A_0 being a characteristic wave amplitude for the free surface) and, equivalently, it is also a measure of the wave spectrum's narrowness around $k = k_0$. The corresponding equations of motion are

$$\partial_t \begin{pmatrix} u \\ \overline{u} \end{pmatrix} = J_2 \begin{pmatrix} \delta_u H \\ \delta_{\overline{u}} H \end{pmatrix} = \varepsilon^{-1} \begin{pmatrix} 0 & -\mathrm{i} \\ \mathrm{i} & 0 \end{pmatrix} \begin{pmatrix} \delta_u H \\ \delta_{\overline{u}} H \end{pmatrix}, \tag{19}$$

where $J_2 = \varepsilon P_2 J_1 P_2^\top$. The extra factor ε in the definition of J_2 reflects the change in symplectic structure associated with the spatial rescaling $x \to X = \varepsilon x$ and defines the time scale of the resulting flows. Further details on these transformations in the context of Hamiltonian models for free-surface flows can be found in [10,13].

5 Hamiltonian Models

The Hamiltonian (16) is also transformed through the changes of variables (17) and (18). The former transformation (17) diagonalizes the quadratic (i.e. linear) part

$$H_2 = \int \overline{z}\,\omega(D) z \,\mathrm{d}x,$$

in terms of normal modes $(z, \overline{z})$ associated with the exact linear dispersion relation

$$\omega(D) = (gG_0)^{1/2} = (g|D|)^{1/2},$$

for deep-water gravity waves. The latter transformation (18) paves the way for the expansion of H in powers of ε. The Taylor expansion (10) of the DNO turns out to be convenient for this purpose.

Due to the multiscale nature of this problem (fast oscillations in x and slow modulation in X), it is important to understand the action of Fourier multiplier operators on multiscale functions [19]. For example, G_0 admits the following asymptotic expansion in ε,

$$\begin{aligned} G_0\left(e^{\mathrm{i}k_0 x}u(X)\right) &= |D_x + \varepsilon D_X|\left(e^{\mathrm{i}k_0 x}u(X)\right) = e^{\mathrm{i}k_0 x}|k_0 + \varepsilon D_X|u(X), \\ &= e^{\mathrm{i}k_0 x}(k_0^2 + 2\varepsilon k_0 D_X + \varepsilon^2 D_X^2)^{1/2}u(X), \\ &= e^{\mathrm{i}k_0 x}(k_0 + \varepsilon D_X + \cdots)u(X), \end{aligned}$$

given that $|D|^2 = D^2$. Hence, we may symbolically write

$$|D_x + \varepsilon D_X| = \left(D_x^2 + 2\varepsilon D_x D_X + \varepsilon^2 D_X^2\right)^{1/2} = |D_x| + \varepsilon |D_x|^{-1} D_x D_X + \cdots$$

Moreover, because our focus is on describing nontrivial dynamics of the wave envelope, the presence of multiple scales needs to be appropriately dealt with. This is a homogenization problem which is addressed in the present Hamiltonian framework via the scale separation lemma of Craig et al. [11,14]. In doing so, terms with fast oscillations essentially homogenize to zero and thus do not contribute to the effective Hamiltonian. This homogenization naturally selects four-wave resonances among all the possible quartic interactions because the corresponding fast oscillations exactly cancel out. We obtain the following principal terms of the water wave Hamiltonian in transformed coordinates, up to fourth order in ε,

$$\begin{aligned} H_2(\eta, \xi) &= \varepsilon \int \overline{u}\,\omega(k_0 + \varepsilon D_X)u \,\mathrm{d}X, \\ H_4(\eta, \xi) &= \frac{\varepsilon^3}{4}\int \left[k_0^3|u|^4 + \frac{3}{2}\varepsilon k_0^2|u|^2\left(\overline{u}D_X u + u\overline{D_X u}\right)\right]\mathrm{d}X, \\ H_4(-\mathrm{i}\,\mathrm{sgn}(D)\eta, \xi) &= -\frac{\varepsilon^3}{4}\int \left[k_0^3|u|^4 + \frac{3}{2}\varepsilon k_0^2|u|^2\left(\overline{u}D_X u + u\overline{D_X u}\right) - 2\varepsilon k_0^2|u|^2|D_X||u|^2\right]\mathrm{d}X. \end{aligned}$$

Note the extra term in $H_4(-\mathrm{i}\,\mathrm{sgn}(D)\eta,\xi)$ as compared to $H_4(\eta,\xi)$, which appears as a result of the normal form transformation. We will comment further on this term in the next section.

5.1 Model with Truncated Dispersion

If we Taylor expand the dispersion relation $\omega(k_0+\varepsilon D_X)$ in ε, and retain terms of order up to $O(\varepsilon^4)$, then the reduced Hamiltonian (16) reads

$$\begin{aligned}
H &= H_2(\eta,\xi)+H_4(\eta,\xi)-H_4(-\mathrm{i}\,\mathrm{sgn}(D)\eta,\xi),\\
&= \frac{\varepsilon}{2}\int \overline{u}\left(\omega_0+\varepsilon\omega_0' D_X+\frac{\varepsilon^2}{2}\omega_0'' D_X^2+\frac{\varepsilon^3}{6}\omega_0''' D_X^3\right)u+\text{c.c.}\\
&\quad+\varepsilon^2 k_0^3|u|^4+\frac{3}{2}\varepsilon^3 k_0^2|u|^2\left(\overline{u}D_X u+u\overline{D_X u}\right)-\varepsilon^3 k_0^2|u|^2|D_X||u|^2\,\mathrm{d}X+O(\varepsilon^5),\\
&= \varepsilon\int \omega_0|u|^2+\varepsilon\omega_0'\,\mathrm{Im}(\overline{u}\partial_X u)+\frac{\varepsilon^2}{2}\omega_0''|\partial_X u|^2+\frac{\varepsilon^2}{2}k_0^3|u|^4\\
&\quad+\frac{\varepsilon^3}{6}\omega_0'''\,\mathrm{Im}\Big[(\overline{\partial_X u})(\partial_X^2 u)\Big]+\frac{3}{2}\varepsilon^3 k_0^2|u|^2\,\mathrm{Im}(\overline{u}\partial_X u)\\
&\quad-\frac{\varepsilon^3}{2}k_0^2|u|^2|D_X||u|^2\,\mathrm{d}X+O(\varepsilon^5),
\end{aligned}\tag{20}$$

where $\omega_0=\omega(k_0)$ and similarly for its derivatives. The initials 'c.c.' stand for the complex conjugate of all the preceding terms on the right-hand side of the equation, and $\mathrm{Im}(\cdot)$ denotes the imaginary part. In (20), we have used the fact that

$$\int \overline{u}D_X u\,\mathrm{d}X=-\int u D_X\overline{u}\,\mathrm{d}X=\int u\overline{D_X u}\,\mathrm{d}X,$$

via integration by parts and, therefore,

$$\int\left(\overline{u}D_X u+u\overline{D_X u}\right)\mathrm{d}X=-\mathrm{i}\int\left(\overline{u}\partial_X u-u\overline{\partial_X u}\right)\mathrm{d}X=2\int\mathrm{Im}(\overline{u}\partial_X u)\,\mathrm{d}X.$$

It follows from (19) that the evolution equation for u is given by

$$\begin{aligned}
\partial_t u &= -\mathrm{i}\varepsilon^{-1}\delta_{\overline{u}}H,\\
&= -\mathrm{i}\omega_0 u-\varepsilon\omega_0'\partial_X u+\mathrm{i}\frac{\varepsilon^2}{2}\omega_0''\partial_X^2 u-\mathrm{i}\varepsilon^2 k_0^3|u|^2 u\\
&\quad+\frac{\varepsilon^3}{6}\omega_0'''\partial_X^3 u-3\varepsilon^3 k_0^2|u|^2\partial_X u+\mathrm{i}\varepsilon^3 k_0^2 u|D_X||u|^2,
\end{aligned}\tag{21}$$

which is a Hamiltonian version of Dysthe's equation for deep-water gravity waves [22], associated with the Hamiltonian (20). This equation describes right-moving waves as indicated by the linear advection term. If we switched the sign in the complex

symplectic decomposition (17) of ξ, we would obtain a model for left-moving waves, with an advection term having the opposite sign.

Note that the prefactors ε^{-1} in (19) and ε in (20) suitably cancel out. The cubic NLS equation is recovered if the $O(\varepsilon^3)$ terms in (21) are neglected. The nonlocal term, which is recognizable by the Fourier multiplier $|D_X| = -\mathrm{i}\,\mathrm{sgn}(D_X)\partial_X$, is a characteristic feature of Dysthe's equation and represents effects from the wave-induced mean flow (also called radiation stress) as pointed out in [13,22]. This nonlocal term naturally arises here from the expansion of $H_4(-\mathrm{i}\,\mathrm{sgn}(D)\eta, \xi)$ and takes a simple explicit form, which is in contrast to previous versions of Dysthe's equation where it is indirectly given by the solution of an auxiliary Laplace problem in a uniform strip [35,36]. This also differs from the approach adopted in [13,14] where mean-flow contributions are assumed *a priori* via correction terms in the transformation (17).

5.2 Moving Reference Frame

The Hamiltonian (20) can be further simplified by subtracting a multiple of the wave action

$$M = \varepsilon \int |u|^2 \,\mathrm{d}X,$$

together with a multiple of the impulse

$$I = \int \eta \partial_x \xi \,\mathrm{d}x = \varepsilon \int \left[k_0|u|^2 + \frac{\varepsilon}{2}\left(\overline{u} D_X u + u\overline{D_X u}\right)\right]\mathrm{d}X + \cdots,$$

yielding

$$\begin{aligned}\widehat{H} &= H - \omega_0' I - \left(\omega_0 - k_0\omega_0'\right) M,\\ &= \varepsilon \int \frac{\varepsilon^2}{2}\omega_0''|\partial_X u|^2 + \frac{\varepsilon^2}{2}k_0^3|u|^4 + \frac{\varepsilon^3}{6}\omega_0''' \,\mathrm{Im}\left[(\overline{\partial_X u})(\partial_X^2 u)\right]\\ &\quad + \frac{3}{2}\varepsilon^3 k_0^2|u|^2\,\mathrm{Im}(\overline{u}\partial_X u) - \frac{\varepsilon^3}{2}k_0^2|u|^2|D_X||u|^2\,\mathrm{d}X.\end{aligned}$$

Because M and I are conserved with respect to the flow of $\widehat{H}$, they Poisson commute with H. This transformation preserves the symplectic structure J_2 and the resulting simplification of (21) reads

$$\begin{aligned}\partial_t u &= -\mathrm{i}\varepsilon^{-1}\delta_{\overline{u}}\widehat{H},\\ &= \mathrm{i}\varepsilon^2\left(\frac{1}{2}\omega_0''\partial_X^2 u - k_0^3|u|^2 u\right) + \varepsilon^3\left(\frac{1}{6}\omega_0'''\partial_X^3 u - 3k_0^2|u|^2\partial_X u + \mathrm{i}k_0^2 u|D_X||u|^2\right),\end{aligned}$$

or equivalently

$$\partial_\tau u = \mathrm{i}\left(\frac{1}{2}\omega_0''\partial_X^2 u - k_0^3|u|^2 u\right) + \varepsilon\left(\frac{1}{6}\omega_0'''\partial_X^3 u - 3k_0^2|u|^2\partial_X u + \mathrm{i}k_0^2 u|D_X||u|^2\right),$$

where $\tau = \varepsilon^2 t$ is the typical slow time scale in the modulation theory for deep-water waves. The subtraction of M from H reflects the property of phase (or gauge) invariance in this approximation, while the subtraction of I is equivalent to changing the coordinate system to a reference frame moving with the group velocity ω_0' in the positive X-direction.

5.3 Model with Exact Dispersion

As suggested in [36], a conceivably better approximation to envelopes of solutions in the modulational regime may be achieved by expanding the nonlinear contributions up to order $O(\varepsilon^4)$ as in Sect. 5.1, while keeping the linear dispersion relation exact. The resulting envelope equation is

$$\partial_t u = -\mathrm{i}\omega(k_0 + \varepsilon D_X)u - \mathrm{i}\varepsilon^2 k_0^3 |u|^2 u - 3\varepsilon^3 k_0^2 |u|^2 \partial_X u + \mathrm{i}\varepsilon^3 k_0^2 u |D_X||u|^2, \tag{22}$$

and the corresponding Hamiltonian is

$$H = \varepsilon \int \overline{u}\, \omega(k_0 + \varepsilon D_X)u + \frac{\varepsilon^2}{2} k_0^3 |u|^4 + \frac{3}{2}\varepsilon^3 k_0^2 |u|^2 \operatorname{Im}(\overline{u}\partial_X u) - \frac{\varepsilon^3}{2} k_0^2 |u|^2 |D_X||u|^2 \,\mathrm{d}X.$$

This model may be viewed as a Hamiltonian version of the modified Dysthe equation that was proposed in [36]. An advantage compared to (21) is its superior linear properties while its numerical solution by a pseudo-spectral method does not require any additional effort since the Fourier multiplier $\omega(k_0 + \varepsilon D_X)$ can be efficiently computed via the fast Fourier transform (FFT).

Comparing the expressions of our new models (21) and (22) to previous Hamiltonian models from [13], the only difference lies in the numerical coefficients of nonlinear terms, otherwise the general form of these equations is the same, with precisely the same types of constitutive terms. Here the nonlinear terms $-\mathrm{i}\varepsilon^2 k_0^3 |u|^2 u$ and $-\varepsilon^3 k_0^2 |u|^2 \partial_X u$ in (21)–(22) have coefficients 1 and 3, respectively, while their coefficients are $1/2$ and $3/2$ in [13]. Note that the sign of these coefficients remains the same. On the other hand, the nonlocal mean-flow term $\mathrm{i}\varepsilon^3 k_0^2 u |D_X||u|^2$ is found to be identical in our present and previous studies. This difference by a factor of 2 for the aforementioned coefficients is a consequence of the normal form transformation since nonlinear terms from $H_4(-\mathrm{i}\,\mathrm{sgn}(D)\eta, \xi)$ and $H_4(\eta, \xi)$ add up together. A careful determination of the envelope equation turns out to be crucial for closely capturing the wave dynamics in the asymptotic regime under consideration, as shown in Sect. 9. Moreover, a refined description of the free surface is equally important for accurate simulations, as discussed in the next section.

6 Reconstruction of the Free Surface

Because equations like (21) only describe the wave envelope, another step is required to reconstruct the actual shape of the free surface from information on the wave envelope. In modulation theory, this reconstruction is usually carried out perturbatively, based on an Ansatz similar to Stokes' expansion, by adding contributions from various harmonics of the wave spectrum. These harmonics are wave modes that correspond to integer multiples of k_0.

Here the reconstruction procedure inverts the transformations associated with our modulational Ansatz and the third-order normal form that eliminates H_3. At any instant t, the conversion of η back to its original definition is governed by Burgers' equation

$$\partial_s \widetilde{\eta} - \widetilde{\eta}\partial_x \widetilde{\eta} = 0, \tag{23}$$

for $s \in (-1, 0]$ with "initial" condition

$$\eta_i(x,t) = \eta(x,t)\big|_{s=-1} = \frac{\varepsilon}{\sqrt{2}} a^{-1}(D)\left[u(X,t)e^{\mathrm{i}k_0 x} + \overline{u}(X,t)e^{-\mathrm{i}k_0 x}\right], \tag{24}$$

where u solves (21). The choice of this initial condition is dictated by the changes of variables (17) and (18), via inversion of P_1 and P_2. Equation (23) may be solved numerically and its solution at $s = 0$ is meant to represent the original physical variable η. Note that η and $\widetilde{\eta}$ are directly related through (13). It is clear from (23) and (24) that the wave dynamics in this modulational regime generates higher-order contributions from lower (i.e. mean flow) and higher harmonics through nonlinear interactions. Corrections by higher harmonics were not taken into account in [13,14]. It is also worth pointing out that the integration time $s \in (-1, 0]$ is well within the existence time

$$s = O\left(\frac{1}{|\partial_x \widetilde{\eta}_i|}\right) = O(\varepsilon^{-1}),$$

before a shock occurs, for Burgers' equation with smooth initial data $\widetilde{\eta}_i$.

As an alternative to the direct numerical solution of (23), a perturbative analytical expression can be obtained in a manner consistent with the Hamiltonian framework, via the Taylor expansion near $s = -1$, i.e.

$$\eta\big|_{s=0} = \eta\big|_{s=-1} + \partial_s \eta\big|_{s=-1} + \frac{1}{2}\partial_s^2 \eta\big|_{s=-1} + \cdots, \tag{25}$$

where

$$\partial_s \eta = \{K_3, \eta\} = \delta_\xi K_3 = \frac{1}{2}|D|\left(-\mathrm{i}\,\mathrm{sgn}(D)\eta\right)^2,$$
$$\partial_s^2 \eta = \partial_s\{K_3, \eta\} = \{K_3, \{K_3, \eta\}\} = \left\{K_3, \delta_\xi K_3\right\},$$

and η at $s = -1$ is given by (24). By analogy with Stokes' expansion for near-monochromatic waves, the first, second and third terms on the right-hand side of (25) include contributions from the first, second and third harmonics respectively.

7 Spatial Dysthe's Equation

7.1 Envelope Equation

To compare with laboratory experiments where time series of the surface elevation are typically recorded by wave gauges at fixed locations along the wave channel, the spatial version of Dysthe's equation has also been considered in numerous studies [27,29,39]. Such a model is derived by switching the role of the X- and t-variables in the envelope equation, with X acting as a time-like variable for wave propagation along the wave channel.

In the absence of a Hamiltonian formulation for the spatial dynamics associated with the basic equations (1)–(4), we follow the standard procedure and apply it to (21). Exploiting the phase invariance, we first introduce

$$v(X,t) = u(X,t)e^{\mathrm{i}\omega_0 t}, \tag{26}$$

to eliminate the linear term $-\mathrm{i}\omega_0 u$, yielding

$$\begin{aligned}\partial_X v = &-2\frac{\omega_0}{g\varepsilon}\partial_t v - \mathrm{i}\varepsilon\frac{g}{4\omega_0^2}\partial_X^2 v - 2\mathrm{i}\varepsilon\frac{\omega_0 k_0^3}{g}|v|^2 v \\ &+ \varepsilon^2\frac{g^2}{8\omega_0^4}\partial_X^3 v - 6\varepsilon^2\frac{\omega_0 k_0^2}{g}|v|^2\partial_X v + 2\mathrm{i}\varepsilon^2\frac{\omega_0 k_0^2}{g}v|D_X||v|^2.\end{aligned} \tag{27}$$

We then substitute all the X-derivatives on the right-hand side with t-derivatives using (27) recursively and retaining terms of suitable order. This leads to

$$\begin{aligned}\partial_X^2 v &= 4\frac{\omega_0^2}{g^2\varepsilon^2}\partial_t^2 v + 4\mathrm{i}\frac{\omega_0}{g^2\varepsilon^2}\partial_t^3 v + 8\mathrm{i}\frac{\omega_0^2 k_0^3}{g^2}\partial_t(|v|^2 v) + \cdots, \\ \partial_X^3 v &= -8\frac{\omega_0^3}{g^3\varepsilon^3}\partial_t^3 v + \cdots,\end{aligned}$$

and after substituting these expressions back in (27), we find

$$\begin{aligned}\partial_X v = &-2\frac{\omega_0}{g\varepsilon}\partial_t v - \frac{\mathrm{i}}{g\varepsilon}\partial_t^2 v - 2\mathrm{i}\varepsilon\frac{\omega_0 k_0^3}{g}|v|^2 v \\ &+ 16\varepsilon\frac{k_0^3}{g}|v|^2\partial_t v + 2\varepsilon\frac{k_0^3}{g}v^2\partial_t\overline{v} + 4\mathrm{i}\varepsilon\frac{k_0^3}{g}v|D_t||v|^2,\end{aligned} \tag{28}$$

or equivalently

$$\partial_x v = -2\frac{\omega_0}{g}\partial_t v - \frac{\mathrm{i}}{g}\partial_t^2 v - 2\mathrm{i}\varepsilon^2\frac{\omega_0 k_0^3}{g}|v|^2 v + 16\varepsilon^2\frac{k_0^3}{g}|v|^2\partial_t v + 2\varepsilon^2\frac{k_0^3}{g}v^2\partial_t\overline{v} + 4\mathrm{i}\varepsilon^2\frac{k_0^3}{g}v|D_t||v|^2,$$

which is the spatial version of (21). Note that $D_t = \mathrm{i}\partial_t$ so that its Fourier symbol is ω. The variable u is recovered by simply inverting (26). Similar to previous spatial Dysthe's equations [27,29,39], there is no $\partial_t^3 v$ term in (28). On the other hand, there is an additional nonlinear term of the form $v^2\partial_t\overline{v}$ and, partly for this reason, the Hamiltonian character of (21) is not inherited by (28). This point, however, is not viewed as detrimental because, as mentioned above, we are only aware of a Hamiltonian formulation for the temporal dynamics of (1)–(4). Moreover, because wave-channel experiments are usually subject to dissipative effects and span relatively short distances of wave propagation [9,27,28], the strict use of a conservative Hamiltonian model may not be particularly relevant to the spatial dynamics.

7.2 Reconstruction of the Free Surface

Since (28) is derived from (21), time series of the surface elevation may be recovered from time series of the wave envelope by referring again to the solution map given by Burgers' flow (23) with initial condition (24), modulo conversion of the x-derivatives to t-derivatives. Accordingly, Eq. (23) becomes

$$\partial_s\widetilde{\eta} + \frac{k_0}{\omega_0}\widetilde{\eta}\partial_t\widetilde{\eta} = 0,$$

for $\widetilde{\eta} = -\mathrm{i}\,\mathrm{sgn}(D)\eta \simeq -\mathrm{i}\,\mathrm{sgn}(D_t)\eta$ by using the approximation $\partial_x\widetilde{\eta} \simeq -(k_0/\omega_0)\partial_t\widetilde{\eta}$. As for (24), it is first approximated via Taylor expansion by

$$\begin{aligned}
\eta(x,t)\big|_{s=-1} &= \frac{\varepsilon}{\sqrt{2}}\left[e^{\mathrm{i}k_0x}a^{-1}(k_0+\varepsilon D_X)u(X,t) + e^{-\mathrm{i}k_0x}a^{-1}(-k_0+\varepsilon D_X)\overline{u}(X,t)\right],\\
&= \frac{\varepsilon}{\sqrt{2}}\left[e^{\mathrm{i}k_0x}\left(a_0^{-1} - \varepsilon a_0' a_0^{-2}D_X\right)u + e^{-\mathrm{i}k_0x}\left(a_0^{-1} + \varepsilon a_0' a_0^{-2}D_X\right)\overline{u}\right] + \cdots,\\
&= \frac{\varepsilon}{\sqrt{2}}a_0^{-1}\left(e^{\mathrm{i}k_0x}u + e^{-\mathrm{i}k_0x}\overline{u}\right) - \frac{\varepsilon^2}{\sqrt{2}}a_0' a_0^{-2}\left(e^{\mathrm{i}k_0x}D_X u + e^{-\mathrm{i}k_0x}\overline{D_X u}\right),\\
&= \sqrt{2}\varepsilon a_0^{-1}\,\mathrm{Re}\left(e^{\mathrm{i}k_0x}u\right) - \sqrt{2}\varepsilon^2 a_0' a_0^{-2}\,\mathrm{Re}\left(e^{\mathrm{i}k_0x}D_X u\right),
\end{aligned}$$

and then converted to

$$\eta(x,t)\big|_{s=-1} = \sqrt{2}\varepsilon a_0^{-1}\,\mathrm{Re}\left(e^{\mathrm{i}(k_0x-\omega_0t)}v\right) - 2\sqrt{2}\varepsilon\frac{\omega_0}{g}a_0' a_0^{-2}\,\mathrm{Re}\left(\mathrm{i}e^{\mathrm{i}(k_0x-\omega_0t)}\partial_t v\right),$$

by virtue of (26) and (28). Again, for notational convenience, $a_0 = a(k_0)$ and $a_0' = a'(k_0)$. We have also used the fact that $a(k_0) = a(-k_0)$ and $a'(-k_0) = -a'(k_0)$, with

$$a'(k) = -\frac{1}{4}\mathrm{sgn}(k)\frac{a(k)}{|k|}.$$

Note that x now plays the role of a parameter in the above reconstruction formula since it would correspond to the location of a wave gauge. The symbol $\mathrm{Re}(\cdot)$ denotes the real part.

8 Stability of Stokes Waves

Both models (21) and (22) admit uniform wavetrain solutions of the form

$$u_0(t) = B_0 e^{-\mathrm{i}(\omega_0 + \varepsilon^2 k_0^3 B_0^2)t}, \tag{29}$$

corresponding to a progressive Stokes wave (B_0 being a positive real constant). These are known to be linearly unstable with respect to sideband perturbations (the so-called modulational or Benjamin–Feir instability). Here we examine this stability problem in the context of (21) and (22).

Considering (21) first, if we insert a perturbed solution of the form

$$u(X,t) = u_0(t)\big[1 + B(X,t)\big],$$

and assume

$$B(X,t) = B_1 e^{\Omega t + \mathrm{i}\lambda X} + B_2 e^{\overline{\Omega} t - \mathrm{i}\lambda X},$$

where $B_1, B_2 \in \mathbb{C}$ and λ denotes sideband wavenumbers, then we find that the condition $\mathrm{Re}(\Omega) \neq 0$ for linear instability implies

$$\alpha = -\omega_0''\lambda^2\left[\omega_0''\lambda^2 + 4k_0^2 B_0^2\,(k_0 - \varepsilon|\lambda|)\right] > 0,$$

which reduces to

$$-\frac{1}{16}gk_0^{-3}\lambda^4 + B_0^2\sqrt{gk_0}\lambda^2\,(k_0 - \varepsilon|\lambda|) > 0, \tag{30}$$

given that

$$\omega''(k) = -\frac{1}{4}\sqrt{g}|k|^{-3/2}.$$

This somewhat straightforward but tedious calculation is similar to those presented in [22,28,35,36]; therefore, we skip details for convenience and only show the final

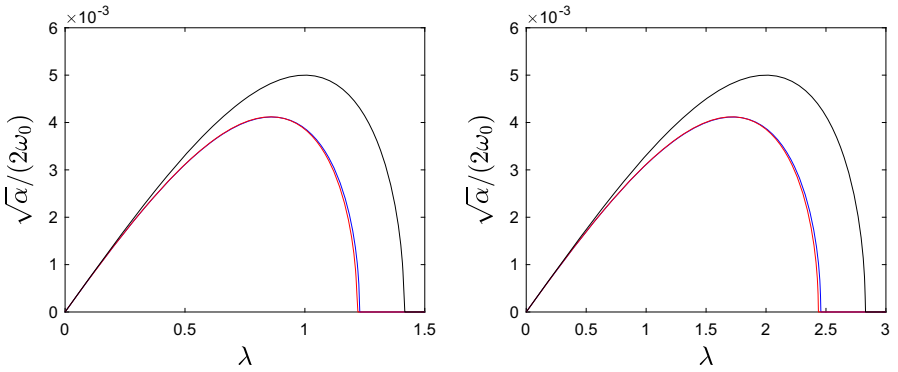

Fig. 1 Growth rates associated with modulational instability for the NLS equation (black line), the envelope equation (21) with truncated dispersion (blue line) and the envelope equation (22) with exact dispersion (red line). Left panel: $(A_0, k_0) = (0.02, 5)$. Right panel: $(A_0, k_0) = (0.01, 10)$ (Color figure online)

result. The criterion based on the cubic NLS equation is recovered if the $O(\varepsilon)$ term is omitted in (30).

Applying the same strategy to (22), we find that sideband instability occurs when

$$\alpha = -\big[\mathcal{D}(\lambda) + \mathcal{D}(-\lambda)\big]^2 + 4\varepsilon^2 k_0^2 B_0^2 \big[\mathcal{D}(\lambda) + \mathcal{D}(-\lambda)\big]\,(k_0 - \varepsilon|\lambda|) > 0, \quad (31)$$

in terms of the exact linear multiplier

$$\mathcal{D}(\lambda) = \omega_0 - \omega(k_0 + \varepsilon\lambda) = \sqrt{gk_0} - \sqrt{g|k_0 + \varepsilon\lambda|}.$$

The slight "Doppler shift" relative to k_0 as induced by the mean flow is clearly noticeable in both (30) and (31).

Figure 1 shows the normalized growth rate

$$\frac{|\,\mathrm{Re}(\Omega)|}{\omega_0} = \frac{\sqrt{\alpha}}{2\omega_0},$$

associated with instability conditions (30) and (31). As a reference, we also plot the normalized growth rate for the cubic NLS equation. Hereafter, all the variables are rescaled to absorb ε back into their definition, and all the equations are non-dimensionalized so that $g = 1$. Two sets of graphs are presented for $(A_0, k_0) = (0.02, 5)$ and $(0.01, 10)$ corresponding to wave steepness $k_0 A_0 = 0.1$. The envelope amplitude in (29) is taken to be

$$B_0 = A_0 \sqrt[4]{\frac{g}{4k_0}}, \quad (32)$$

according to (17) and (18). We see that the curves have a typical lobate shape and, as expected, instability occurs at sideband wavenumbers λ near zero. As a result of the Doppler shift, the growth rates for (21) and (22), whose curves are almost

indistinguishable at this graphical scale, are lower than that for the NLS equation. However, overall, all three models give similar predictions on modulational instability. In particular, they predict maximum instability (i.e. maximum growth rate) at $\lambda \simeq 1$ for $(A_0, k_0) = (0.02, 5)$ and at $\lambda \simeq 2$ for $(A_0, k_0) = (0.01, 10)$.

9 Numerical Results

In this section, we show numerical simulations to illustrate the performance of Hamiltonian envelope equations, as established by the present approach, in comparison with the full equations (6) and (7). We focus here on time-domain simulations based on (21) and, as an additional test, we also compare them to predictions by the "classical" non-Hamiltonian Dysthe's equation

$$\begin{aligned}\partial_t A = &-\frac{\omega_0}{2k_0}\partial_x A - \mathrm{i}\frac{\omega_0}{8k_0^2}\partial_x^2 A - \frac{\mathrm{i}}{2}\omega_0 k_0^2 |A|^2 A \\ &+ \frac{\omega_0}{16k_0^3}\partial_x^3 A - \frac{3}{2}\omega_0 k_0 |A|^2 \partial_x A - \frac{1}{4}\omega_0 k_0 A^2 \partial_x \overline{A} - \mathrm{i}k_0 A \partial_x \Phi, \end{aligned} \tag{33}$$

where the wave-induced mean flow is represented by

$$\Phi = \frac{\mathrm{i}}{2}\omega_0 \,\mathrm{sgn}(D)|A|^2, \qquad \partial_x \Phi = -\frac{1}{2}\omega_0 |D||A|^2.$$

In this context [30,35], the surface elevation and velocity potential are reconstructed perturbatively as

$$\begin{aligned}\eta(x,t) = &\frac{1}{2\omega_0}\partial_x \Phi + A\cos(\theta) + \frac{1}{2}k_0 A^2 \cos(2\theta) + \frac{1}{2}A(\partial_x A)\sin(2\theta) \\ &+ \frac{3}{8}k_0^2 A^3 \cos(3\theta) + \cdots, \\ \varphi(x,y,t) = &\Phi + \frac{\omega_0}{k_0} A\, e^{k_0 y}\sin(\theta) + \frac{\omega_0}{2k_0^2}(\partial_x A)\, e^{k_0 y}\cos(\theta) - \frac{1}{8}\omega_0 k_0 |A|^2 A\, e^{k_0 y}\sin(\theta) \\ &- \frac{3\omega_0}{8k_0^3}(\partial_x^2 A)\, e^{k_0 y}\sin(\theta) + \cdots, \end{aligned} \tag{34}$$

where the fast dynamics is encoded in the phase $\theta = k_0 x - \omega_0 t$. These formulas include contributions from up to the third harmonics, as typically reported in the literature. For convenience, Eqs. (33) and (34) are expressed in terms of unscaled variables without explicit appearance of the perturbation parameter.

The full equations (6) and (7) are solved numerically via a high-order spectral approach [17]. They are discretized in space by a pseudo-spectral method based on the FFT. The computational domain spans the interval $0 \le x \le L$ with periodic boundary conditions and is divided into a regular grid of N collocation points. The DNO is computed via its series expansion (10) but, by analyticity, a small number M of terms is sufficient to achieve highly accurate results. The number $M = 6$ is

selected based on previous extensive tests [9,24,37]. Time integration of (6) and (7) is carried out in the Fourier space so that the linear terms can be solved exactly by the integrating factor technique. The nonlinear terms are integrated in time using a fourth-order Runge–Kutta scheme with constant step Δt.

Naturally, the same numerical methods are used for space discretization and time integration of the envelope equations (21) and (33), and the same spatial and temporal resolutions are specified for their numerical solutions. The reader may refer to [14] for more details on such simulations. For (21), the surface elevation is reconstructed via (23)–(24), while Eq. (34) is used for (33). The same numerical strategy applies to these reconstruction formulas. In particular, Burgers' equation (23) is integrated over s using the same step size $\Delta s = \Delta t$. We point out that, although the surface reconstruction for (21) requires solving a nonlinear PDE, this computation is relatively straightforward and is not necessarily performed at each instant t (only when data on the free surface are requested, say for plotting purposes). Moreover, because this PDE is solved over a relatively short interval $s \in (-1, 0]$, the associated cost is insignificant. The whole computation in this case (i.e. solving for the wave envelope and reconstructing the surface elevation) can be produced by a single self-contained computer code. Note that, when Eq. (21) is solved numerically, the linear term $-\mathrm{i}\omega_0 u$ may be dealt with by either incorporating the coefficient $-\mathrm{i}\omega_0$ into the integrating factor as part of the time integration scheme, or by inserting the phase shift $-\mathrm{i}\omega_0 t$ in (24) as part of the surface reconstruction procedure, similar to (34). We found identical results either way.

For these numerical tests, we have in mind the stability problem that was analyzed in the previous section. Given a value of the wave steepness $k_0 A_0$, the initial conditions for (21) and (33) are taken to be

$$u(x, 0) = B_0\big[1 + 0.1\cos(\lambda x)\big], \qquad A(x, 0) = A_0\big[1 + 0.1\cos(\lambda x)\big],$$

respectively, so as to represent a perturbed Stokes wave, with A_0 and B_0 being related through (32). We compare these two weakly nonlinear models by testing their individual performance against the full equations (6) and (7). Because u and A do not exactly describe the same physical quantity, and because the corresponding reconstruction procedures are not exactly identical, it is important to specify suitable initial conditions on η and ξ for (6)–(7), depending on whether these equations are compared to our new Hamiltonian model (21) or to the classical Dysthe's equation (33). This is accomplished using (15) together with $u(x, 0)$ on the one hand and using (34) together with $A(x, 0)$ on the other hand. In doing so, the initial surface profile for (6)–(7) exactly coincides with that for either (21) or (33).

In all the following simulations, the length of the computational domain is chosen to be $L = 2\pi$; hence, the discrete Fourier modes are integers. The spatial and temporal resolutions are set to $\Delta x = 0.012$ ($N = 512$) and $\Delta t = 0.005$, respectively. We first consider a case of "small" initial data with $A_0 = 0.01$, $k_0 = 5$ and $\lambda = 1$ (hence $\varepsilon = 0.05$), and examine the wave dynamics over a long time up to $t = 8000 = O(\varepsilon^{-3})$. This corresponds to the timescale over which the Dysthe's approximation with such initial data is supposed to be valid. Figure 2 shows the two individual comparisons on η at $t = 8000$. With such a mild perturbation, the modulational instability has not yet started to develop. In both cases, the wave profiles remain close to their initial

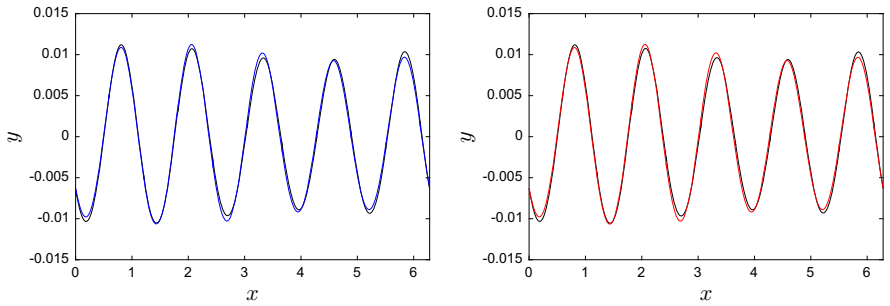

Fig. 2 Comparison on η between the fully and weakly nonlinear solutions at $t = 8000$ for $A_0 = 0.01$, $k_0 = 5$ and $\lambda = 1$. Left panel: Hamiltonian model (21) in blue. Right panel: classical Dysthe's equation (33) in red. The black curve represents the fully nonlinear solution of (6) and (7) (Color figure online)

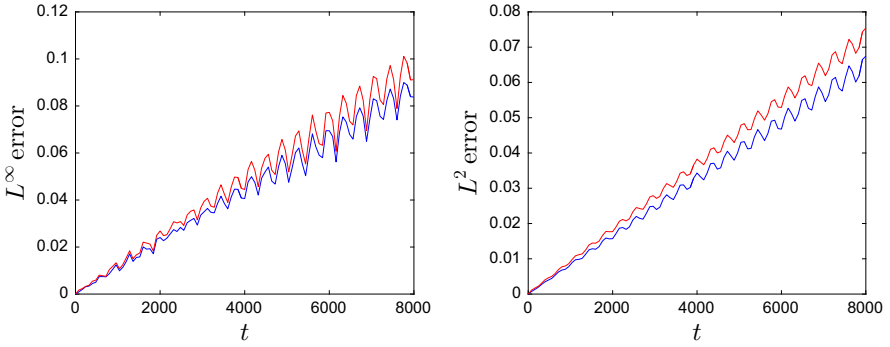

Fig. 3 Relative errors on η between the fully and weakly nonlinear solutions for $A_0 = 0.01$, $k_0 = 5$ and $\lambda = 1$. The blue curve represents the Hamiltonian model (21) while the red curve represents the classical Dysthe's equation (33). Left panel: L^∞ error. Right panel: L^2 error (Color figure online)

configuration and, as a result, discrepancies remain negligible. At this graphical scale, both sets of wave profiles look identical. A more quantitative assessment is provided in Fig. 3 which plots the time evolution of the relative L^∞ and L^2 errors

$$\frac{\|\eta_f - \eta_w\|_\infty}{\|\eta_f\|_\infty}, \qquad \frac{\|\eta_f - \eta_w\|_2}{\|\eta_f\|_2}, \tag{35}$$

on η between the fully (η_f) and weakly (η_w) nonlinear solutions. The magnitude of these errors confirm that both models perform very well in this case, with the predictions from (21) being slightly better than those from (33). This may be expected since the surface reconstruction for (21) is a non-perturbative calculation that is done numerically, while that for (33) is a perturbative calculation which includes corrections from up to the third harmonics only.

We now turn our attention to two cases of "rougher" initial data, one with $A_0 = 0.02$, $k_0 = 5$, $\lambda = 1$ and the other with $A_0 = 0.01$, $k_0 = 10$, $\lambda = 2$. In both cases, the wave steepness $\varepsilon = 0.1$ is larger than in the previous test and, accordingly, the wave dynamics is more prone to modulational instability. The perturbation wavenumber λ

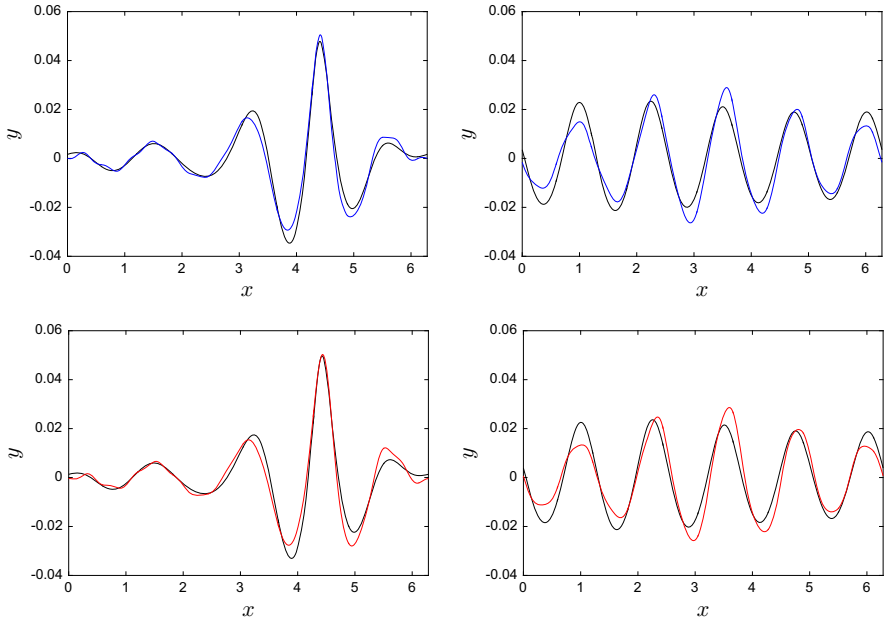

Fig. 4 Comparison on η between the fully and weakly nonlinear solutions at $t = 370$ (left panels) and $t = 820$ (right panels) for $A_0 = 0.02$, $k_0 = 5$ and $\lambda = 1$. Top panels: Hamiltonian model (21) in blue. Bottom panels: classical Dysthe's equation (33) in red. The black curve represents the fully nonlinear solution of (6) and (7) (Color figure online)

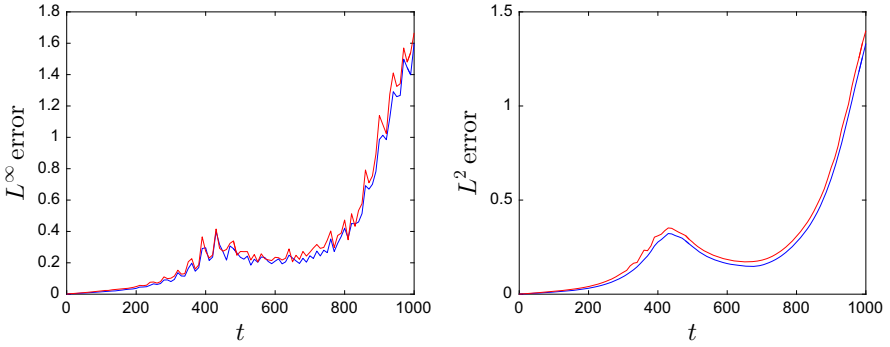

Fig. 5 Relative errors on η between the fully and weakly nonlinear solutions for $A_0 = 0.02$, $k_0 = 5$ and $\lambda = 1$. The blue curve represents the Hamiltonian model (21) while the red curve represents the classical Dysthe's equation (33). Left panel: L^∞ error. Right panel: L^2 error (Color figure online)

is chosen in such a way that the most unstable mode as predicted by stability analysis would be promptly excited (see Sect. 8). Comparison of (21) and (33) with (6)–(7) is presented in Figs. 4, 5 and 6, 7 for these two cases. As expected, it does not take long for the Stokes wave to become unstable and a cycle of modulation–demodulation seems to repeat itself over time. The free surface undergoes strong distortions during this process and, as a consequence, the model's performance gradually deteriorates. Due

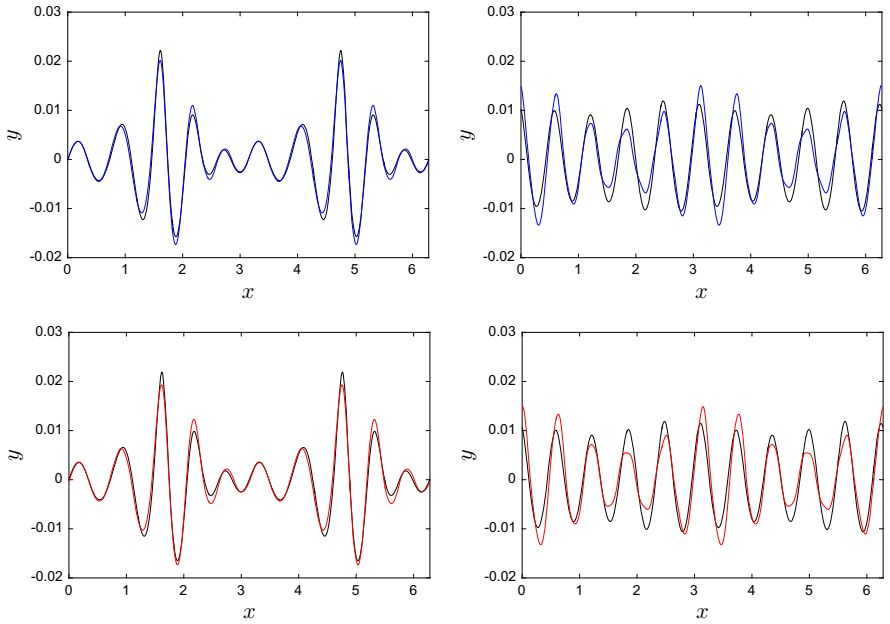

Fig. 6 Comparison on η between the fully and weakly nonlinear solutions at $t = 240$ (left panels) and $t = 590$ (right panels) for $A_0 = 0.01$, $k_0 = 10$ and $\lambda = 2$. Top panels: Hamiltonian model (21) in blue. Bottom panels: classical Dysthe's equation (33) in red. The black curve represents the fully nonlinear solution of (6) and (7) (Color figure online)

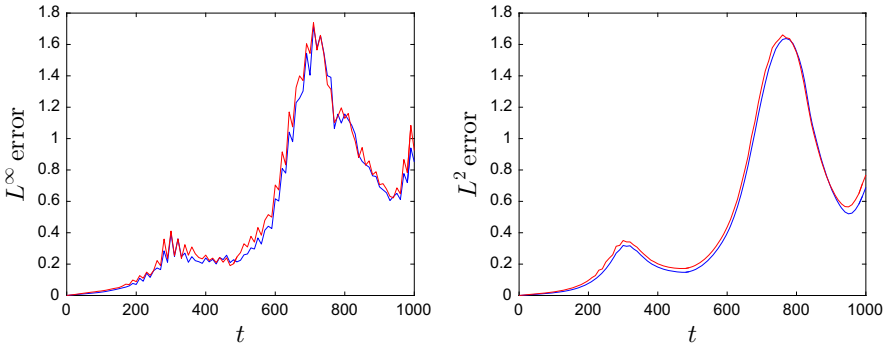

Fig. 7 Relative errors on η between the fully and weakly nonlinear solutions for $A_0 = 0.01$, $k_0 = 10$ and $\lambda = 2$. The blue curve represents the Hamiltonian model (21) while the red curve represents the classical Dysthe's equation (33). Left panel: L^∞ error. Right panel: L^2 error (Color figure online)

to the weakly nonlinear character of (21) and (33), the rougher the initial condition, the sooner discrepancies arise and the more severe they get. Excitation of the first and second sideband modes is clearly revealed on the snapshots at $t = 370$ (Fig. 4) and $t = 240$ (Fig. 6), respectively, near the times of maximum wave growth. We note that, although the classical Dysthe's solution agrees well with the fully nonlinear solution around the dominant wave crest at $t = 370$, it does not do so well at other

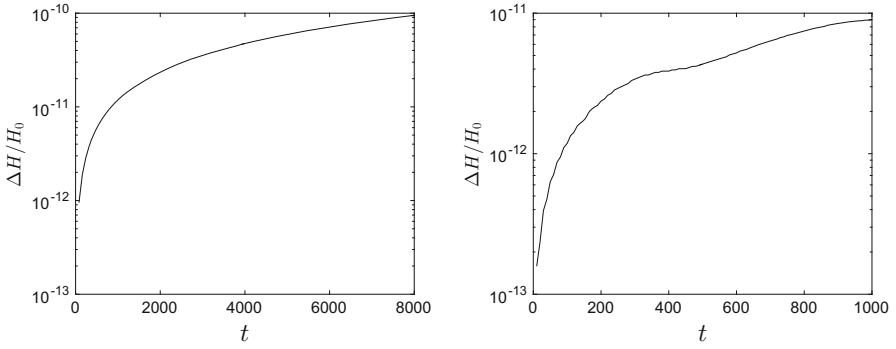

Fig. 8 Relative error on H for the Hamiltonian model (21). Left panel: $A_0 = 0.01$, $k_0 = 5$ and $\lambda = 1$. Right panel: $A_0 = 0.02$, $k_0 = 5$ and $\lambda = 1$

locations like the neighboring crests and troughs. Overall, both models give similar results though again the relative L^∞ and L^2 errors in Figs. 5 and 7 tend to slightly favor our Hamiltonian model (21) together with the reconstruction algorithm based on (23).

Aside from these small quantitative discrepancies, the fact that in all three cases Eq. (21) qualitatively displays the same pattern of wave instability as for the classical Dysthe's equation and the full Euler's equations (at least over the time scales under consideration) provides further validation for our stability results and hence our modulational approach.

Finally, the time evolution of the relative error

$$\frac{\Delta H}{H_0} = \frac{|H - H_0|}{H_0},$$

on energy (20) associated with the Hamiltonian model (21) is illustrated in Fig. 8 for $A_0 = 0.01$ and 0.02 (with $k_0 = 5$ and $\lambda = 1$). Integrals in (20) and in the L^2 norm (35) are computed via the trapezoidal rule over the periodic cell $[0, L]$. The reference value H_0 denotes the initial value of (20) at $t = 0$. Overall, H is very well conserved in both cases, despite a gradual loss of accuracy over time that is likely due to accumulation of numerical errors. These results can certainly be improved by specifying smaller grid sizes in space and time. We recall that, unlike the classical Dysthe's Eq. (33), our new model (21) possesses a well-defined Hamiltonian structure that is consistent with the Hamiltonian formulation of the full Eqs. (6)–(7). As a consequence, it admits a conserved "energy" (20) whose counterpart for (33) is not known.

10 Conclusions

We have derived a new Hamiltonian version of Dysthe's equation for two-dimensional weakly modulated gravity waves on deep water. From the basic Hamiltonian formulation of the water wave problem, our derivation makes use of a Birkhoff normal form transformation to eliminate all non-resonant cubic terms, as recently proposed

by Craig and Sulem [18], in combination with a set of canonical transformations and homogenization techniques, as previously introduced by Craig et al. [13,14], to obtain a reduced model for the wave envelope. It follows from these transformations that the envelope equation automatically inherits a symplectic structure and a conserved energy. We have also provided extensions of this Hamiltonian Dysthe's equation to cases where exact linear dispersion is retained and where the model is rewritten in an alternate spatial form.

We have then conducted a Benjamin–Feir stability analysis for uniform wavetrains (i.e. Stokes waves) and checked its predictions against numerical simulations of our model. These were compared to computations based on the classical Dysthe's equation and the full Euler's equations. In this regard, we have also paid attention to the post-processing step of reconstructing the free surface from the wave envelope. Exploiting the normal form transformation, we have developed a new non-perturbative approach for surface reconstruction which involves solving a nonlinear PDE and incorporates higher order harmonic contributions in a natural way. By doing so, we have obtained very good agreement under various wave conditions. Our Hamiltonian method seems to perform slightly better than the standard procedure associated with Dysthe's equation.

Looking ahead, it would be of interest to extend the present method to the situation of constant finite depth with possibly surface tension, as well as to the three-dimensional setting. High-order terms in the model equations are expected to be more complicated in these cases, and nontrivial behavior may be observed for certain values of the physical parameters [1,2]. For example, it is well known that the nonlinear term of the NLS equation for surface gravity waves on finite depth changes sign at the critical depth $k_0 h \simeq 1.363$, with consequences on the Benjamin–Feir instability [19]. In our approach, the third-order normal form transformation for the finite-depth case can be written explicitly but does not have a simple form. This will be the subject of subsequent work.

Acknowledgements This paper was almost completed a few weeks before Walter Craig passed away. It is with great sadness that we lost our long-time collaborator and dear friend. We will forever be grateful to Walter for his inspiration and friendship. W. C. was partially supported by the Canada Research Chairs Program and Natural Sciences and Engineering Research Council of Canada through grant 238452–16. P. G. is partially supported by the National Science Foundation through Grant no. DMS–1615480. C. S. is partially supported by the Natural Sciences and Engineering Research Council of Canada through Discovery Grant 2018-04536 and a Killam Research Fellowship from the Canada Council for the Arts.

Compliance with ethical standards

Conflict of interest The authors declare that they have no conflict of interest.

References

1. Ablowitz, M.J., Segur, H.: On the evolution of packets of water waves. J. Fluid Mech. **92**, 691–715 (1979)
2. Ablowitz, M.J., Segur, H.: Solitons and the Inverse Scattering Transform, Studies in Applied and Numerical Mathematics. SIAM, Philadelphia (1981)

3. Bambusi, D.: Birkhoff normal form for some nonlinear PDEs. Commun. Math. Phys. **234**, 253–285 (2003)
4. Bambusi, D.: A Birkhoff normal form theorem for some semilinear PDEs. Hamiltonian Dynamical Systems and Applications, NATO Science for Peace and Security Series, pp. 213–247. Springer, Dordrecht (2008)
5. Berti, M., Feola, R., Pusateri, F.: Birkhoff normal form and long time existence for periodic gravity water waves. arXiv:1810.11549
6. Coifman, R., Meyer, Y.: Nonlinear harmonic analysis and analytic dependence. Proc. Sympos. Pure Math. **43**, 71–78 (1985)
7. Craig, W.: Birkhoff normal forms for water waves. Contemp. Math. **200**, 57–74 (1996)
8. Craig, W., Groves, M.D.: Hamiltonian long-wave approximations to the water-wave problem. Wave Motion **19**, 367–389 (1994)
9. Craig, W., Guyenne, P., Hammack, J., Henderson, D., Sulem, C.: Solitary water wave interactions. Phys. Fluids **18**, 057106 (2006)
10. Craig, W., Guyenne, P., Kalisch, H.: Hamiltonian long-wave expansions for free surfaces and interfaces. Commun. Pure Appl. Math. **58**, 1587–1641 (2005)
11. Craig, W., Guyenne, P., Nicholls, D.P., Sulem, C.: Hamiltonian long-wave expansions for water waves over a rough bottom. Proc. R. Soc. Lond. A **461**, 839–873 (2005)
12. Craig, W., Guyenne, P., Sulem, C.: Water waves over a random bottom. J. Fluid Mech. **640**, 79–107 (2009)
13. Craig, W., Guyenne, P., Sulem, C.: A Hamiltonian approach to nonlinear modulation of surface water waves. Wave Motion **47**, 552–563 (2010)
14. Craig, W., Guyenne, P., Sulem, C.: Hamiltonian higher-order nonlinear Schrödinger equations for broader-banded waves on deep water. Eur. J. Mech. B/Fluids **32**, 22–31 (2012)
15. Craig, W., Guyenne, P., Sulem, C.: The surface signature of internal waves. J. Fluid Mech. **710**, 277–303 (2012)
16. Craig, W., Schanz, U., Sulem, C.: The modulational regime of three-dimensional water waves and the Davey–Stewartson system. Ann. Inst. Henri Poincaré **14**, 615–667 (1997)
17. Craig, W., Sulem, C.: Numerical simulation of gravity waves. J. Comput. Phys. **108**, 73–83 (1993)
18. Craig, W., Sulem, C.: Mapping properties of normal forms transformations for water waves. Boll. Unione Mat. Ital. **9**, 289–318 (2016)
19. Craig, W., Sulem, C., Sulem, P.-L.: Nonlinear modulation of gravity waves: a rigorous approach. Nonlinearity **5**, 497–522 (1992)
20. Düll, W.-P., Schneider, G., Wayne, C.E.: Justification of the nonlinear Schrödinger equation for the evolution of gravity driven 2D surface water waves in a canal of finite depth. Arch. Ration. Mech. Anal. **220**, 543–602 (2016)
21. Dyachenko, A.I., Kachulin, D.I., Zakharov, V.E.: Super compact equation for water waves. J. Fluid Mech. **828**, 661–679 (2017)
22. Dysthe, K.B.: Note on a modification to the nonlinear Schrödinger equation for application to deep water waves. Proc. R. Soc. Lond. A **369**, 105–114 (1979)
23. Gramstad, O., Trulsen, K.: Hamiltonian form of the modified nonlinear Schrödinger equation for gravity waves on arbitrary depth. J. Fluid Mech. **670**, 404–426 (2011)
24. Guyenne, P., Nicholls, D.P.: A high-order spectral method for nonlinear water waves over moving bottom topography. SIAM J. Sci. Comput. **30**, 81–101 (2007)
25. Guyenne, P., Nicholls, D.P., Sulem, C. (eds.): Hamiltonian Partial Differential Equations and Applications. Fields Institute Communications, vol. 75. Springer, New York (2015)
26. Krasitskii, V.P.: On reduced equations in the Hamiltonian theory of weakly nonlinear surface waves. J. Fluid Mech. **272**, 1–20 (1994)
27. Lo, E., Mei, C.C.: A numerical study of water-wave modulation based on a higher-order nonlinear Schrödinger equation. J. Fluid Mech. **150**, 395–416 (1985)
28. Segur, H., Henderson, D., Carter, J., Hammack, J., Li, C.-M., Pheiff, D., Socha, K.: Stabilizing the Benjamin–Feir instability. J. Fluid Mech. **539**, 229–271 (2005)
29. Shemer, L., Kit, E., Jiao, H.: An experimental and numerical study of the spatial evolution of unidirectional nonlinear water-wave groups. Phys. Fluids **14**, 3380–3390 (2002)
30. Slunyaev, A.V.: Numerical simulation of "limiting" envelope solitons of gravity waves on deep water. JETP **109**, 676–686 (2009)

31. Stiassnie, M.: Note on the modified nonlinear Schrödinger equation for deep water waves. Wave Motion **6**, 431–433 (1984)
32. Sulem, C., Sulem, P.-L.: The Nonlinear Schrödinger Equation: Self-Focusing and Wave Collapse. Series in Mathematical Sciences, vol. 139. Springer, New York (1999)
33. Totz, N.: A justification of the modulation approximation to the 3D full water wave problem. Commun. Math. Phys. **335**, 369–443 (2015)
34. Totz, N., Wu, S.: A rigorous justification of the modulation approximation to the 2D full water wave problem. Commun. Math. Phys. **310**, 817–883 (2012)
35. Trulsen, K., Dysthe, K.B.: A modified nonlinear Schrödinger equation for broader bandwidth gravity waves on deep water. Wave Motion **24**, 281–289 (1996)
36. Trulsen, K., Kliakhandler, I., Dysthe, K.B., Velarde, M.G.: On weakly nonlinear modulation of waves on deep water. Phys. Fluids **12**, 2432–2437 (2000)
37. Xu, L., Guyenne, P.: Numerical simulation of three-dimensional nonlinear water waves. J. Comput. Phys. **228**, 8446–8466 (2009)
38. Zakharov, V.E.: Stability of periodic waves of finite amplitude on the surface of a deep fluid. J. Appl. Mech. Tech. Phys. **9**, 190–194 (1968)
39. Zhang, H.D., Guedes Soares, C., Onorato, M.: Modelling of the spatial evolution of extreme laboratory wave heights with the nonlinear Schrödinger and Dysthe equations. Ocean Eng. **89**, 1–9 (2014)